

Thermodynamics of the low-temperature structural transition in rare-earth-doped $\text{La}_{2-x}\text{Sr}_x\text{CuO}_4$

Ralph Werner*

Institut für Physik, Universität Dortmund, D-44221 Dortmund, Germany

M. Hücker and B. Büchner

II. Physikalisches Institut, Universität zu Köln, D-50937 Köln, Germany

(October 23, 2018)

The Sr concentration dependence of the structural transition from the orthorhombic into the tetragonal low-temperature phase in rare-earth-doped ($R = \text{Nd, Eu}$) $\text{La}_{2-x-y}\text{Sr}_x\text{R}_y\text{CuO}_4$ has been studied in detail. Independently of the rare earth concentration the transition temperature is strongly reduced at $x \sim 0.05$. We give a qualitative argument that the effect can be attributed to the Coulomb repulsion between doped carriers. We find the enthalpy jump at the low-temperature transition to scale transition temperature between the high-temperature tetragonal and the orthorhombic phase. This effect can be understood in terms of a Landau expansion.

I. INTRODUCTION

The observation of static stripe correlations in $\text{La}_{1.475}\text{Nd}_{0.40}\text{Sr}_{0.12}\text{CuO}_4$ renewed the interest in rare-earth-doped (R) lanthanide copper oxides.¹ The observation of static stripes is induced by a low-temperature (LT) structural transition from a low-temperature orthorhombic (LTO) to a tetragonal low-temperature phase (LTT). A static superlattice structure appears close to the structural transition, which can be accounted for by the appearance of evenly spaced static stripes.²⁻⁴ On the other hand, the incommensurability of the magnetic 2D correlations seen in neutron scattering experiments^{5,6} with $\text{La}_{2-x}\text{Sr}_x\text{CuO}_4$ can be viewed as a consequence of the formation of charged stripes separating antiferromagnetically ordered domains, because the magnetic order parameter suffers an antiphase jump across such a domain wall.^{7,8} The Sr dependence of the antiferromagnetic incommensurability is consistent with the gathering of the doped carriers in domain walls.⁹ In $\text{La}_{2-x}\text{Sr}_x\text{CuO}_4$ the domain walls are expected to be very mobile objects,¹⁰ rendering the experimental proof of their existence extremely difficult.

The antiferromagnetic incommensurability is assumed to be the same in the LTO and LTT phase.⁹ Since in the LTT phase the incommensurability can be accounted for by the static stripes the obvious conclusion is that in the LTO phase the incommensurability may be caused by dynamical stripes.¹⁰ A better understanding of the influence of the LTO-LTT transition on the electronic system is thus desirable.

The LTO-LTT transition is invoked by further rare-earth (R) doping of $\text{La}_{2-x-y}\text{Sr}_x\text{R}_y\text{CuO}_4$.¹¹ In both phases the CuO_6 octahedra are tilted with respect to the crystallographic axes by an angle $\Phi < 5^\circ$. In the LTO phase the tilt axis is parallel $[110]_{\text{HTT}}$ and rotates discontinuously by $\theta = 45^\circ$ towards the $[100]_{\text{HTT}}$ direction at the transition into the LTT phase (we use the notation of the undistorted tetragonal high-temperature phase HTT). Note that the tilt angle Φ is roughly the same in the LTO and the LTT phase while the different directions of the tilt produce different buckling pattern of the CuO_2 plane. The transition temperature is of the order of $T_{\text{LT}} \sim 100$ K.

In this work we investigate both Eu and Nd doped $\text{La}_{2-x}\text{Sr}_x\text{CuO}_4$. It is worthwhile to mention that the LT phase is the more stable the smaller the R element, which renders the europium samples advantageous. Especially for Nd doped $\text{La}_{2-x}\text{Sr}_x\text{CuO}_4$ for $x < 0.10$ the LTO-LTT transition becomes a sequence of two transformations.¹¹ First at T_{LT} a discontinuous transition from the LTO into the intermediate $Pccn$ phase takes place followed by a continuous development into the LTT phase. The $Pccn$ phase is characterized by a rotation of the tilt axis which is less than 45° . In the Eu-doped samples the LT transition occurs at higher temperatures ($T_{\text{LT}} \sim 130$ K) and the appearance of the $Pccn$ phase is strongly reduced to Sr contents smaller $x \sim 0.07$. Yet, at lower temperatures (~ 50 K-60 K) all samples are in the LTT phase making a direct comparison possible. The generic phase diagram is shown in Fig. 1.

The structural data have been collected on polycrystalline material of Nd and Eu doped $\text{La}_{2-x}\text{Sr}_x\text{CuO}_4$. The samples used in this study have been prepared by a standard solid state reaction described by Breuer *et al.*¹² Those with small Sr content where annealed in N_2 atmosphere at temperatures between 550° and 625° for several days to remove excess oxygen.

*Present address: Physics Department, Brookhaven National Laboratory, Upton, NY 11973-5000, USA.

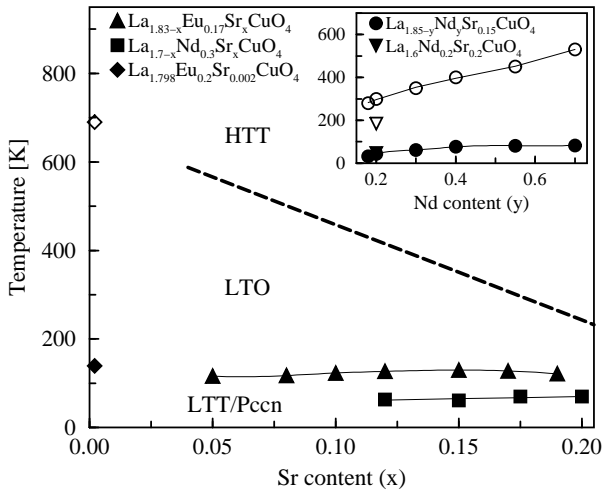


FIG. 1. Generic phase diagram obtained from the doping dependent transition temperatures for different R concentrations. Open symbols mark HTT-LTO transition temperatures T_{HT} , the broken line marks the HTT-LTO transition for the $Eu_{0.17}$ (\circ) and the $Nd_{0.3}$ (\square) samples determined in earlier work. (The stochiometry has been chosen such that both the $Eu_{0.17}$ and $Nd_{0.3}$ samples have the same T_{HT} .) The filled symbols show the LTO-LTT transitions T_{LT} . The figure shows the Sr dependence of the transitions, the inset the Nd dependence. Thin lines are guides to the eye.

II. CHARACTERISTIC MINIMUM OF THE DOPING DEPENDENT LTO-LTT TRANSITION

In Fig. 2 we present the Sr concentration dependence of T_{LT} obtained from four series of samples with different Nd and Eu concentrations. The data clearly shows that T_{LT} is a nonmonotonous function of the hole content x . T_{LT} varies between 70 K ($x = 0$) and 153 K ($x = 0.002$) for the samples with extremely small Sr content, then strongly decreases by about 20 K to 30 K showing a local minimum around $x \sim 0.05$, and increases for higher Sr concentrations. The transition temperatures reach a plateau at intermediate doping $x > 1/8$ and fall off again when approaching the HTT-LTO transition line shown in Fig. 1. Note that this decrease is not for all samples within the plot range of Fig. 2.

The minimum in the underdoped region centered around $x \sim 0.05$ is characteristic for all R doping. It is straightforward to attribute this universal behavior to the same origin. The Sr doping strongly effects the electron configuration of the CuO_4 planes. Also, an explanation of the nonmonotonous behavior by sterical reasons fails because no comparable Sr dependence is observed for other relevant lattice parameters.^{13,14} Therefore, a correlation with electronic properties is very likely.⁴

We limit ourselves to present a qualitative argument showing that the Coulomb repulsion between doped carriers is a possible origin of the characteristic minimum

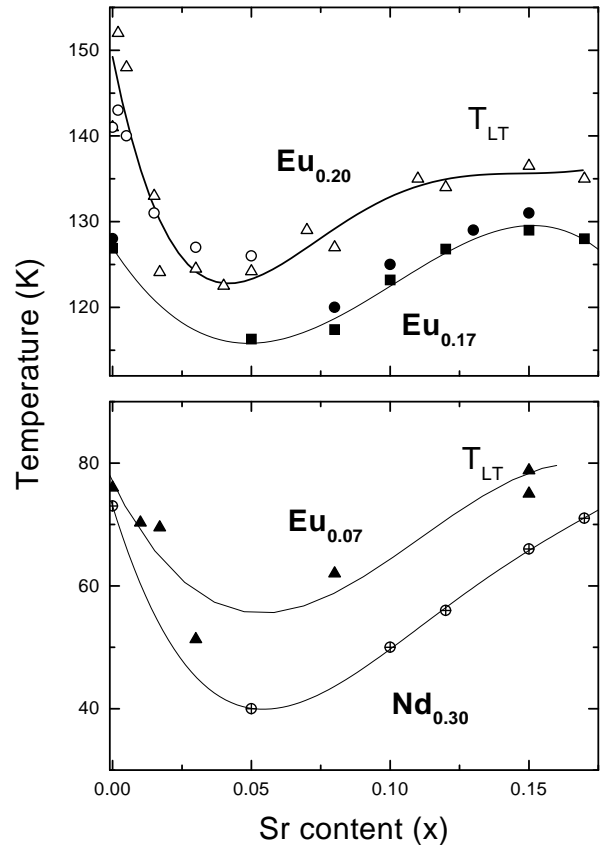


FIG. 2. LTO-LTT transition temperature T_{LT} in $La_{2-x-y}Sr_xR_yCuO_4$ versus Sr content for four series of samples as symbolized by: $Eu_{0.20}$: \circ x-ray, \triangle χ ; $Eu_{0.17}$: \bullet x-ray, \square c_p ; $Eu_{0.07}$: \triangle χ ; $Nd_{0.30}$: \oplus x-ray. (Eu LTO-LTT and LTO-Pccn); (Nd LTO-Pccn)

of T_{LT} . In the LTT phase we may assume the holes to form static stripes. From the position of the incommensurate magnetic and charge peaks of the neutron scattering data of the $La_{1.48}Nd_{0.4}Sr_{0.12}CuO_4$ compound one can conclude that the stripes carry one hole per two copper sites.¹ From the incommensurability measured for other Sr concentrations⁹ we can assume that the half filled case (1/2 hole per copper) is generic for pinned charged stripes. The resulting static hole configuration is shown in Fig. 3 a).

In the LTO phase the hole configuration is still controversial. The picture of a uniform charge distribution can be modeled by a static square lattice formed by the holes as shown in Fig. 3 c). Fluctuating stripes are represented by a zig-zag configuration of the holes as shown in Fig. 3 b) accounting for the larger mean distance between holes due to fluctuations. Configuration b) may also be realized in the LTT phase by allowing fluctuations around the static position of the stripe.

We now compare the corresponding Madelung energies

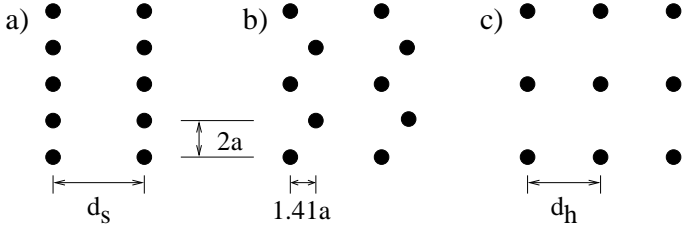


FIG. 3. Hole configurations considered. a) Half filled static stripes in the LTT phase. b) Zig-zag modulation of dynamic stripes with larger mean distances between holes in the LTO phase. c) Homogeneous LTO configuration. The distances $d_h = \sqrt{x}^{-1}$ and $d_s = (2x)^{-1}$ for the Sr concentration x are given in units of the lattice spacing a .

in the LTO and LTT phase.

$$\Delta E_c = x \sum_{\mathbf{r}_{\text{LTO}}} \frac{e^{-\lambda|\mathbf{r}_0 - \mathbf{r}_{\text{LTO}}|}}{|\mathbf{r}_0 - \mathbf{r}_{\text{LTO}}|} - x \sum_{\mathbf{r}_{\text{LTT}}} \frac{e^{-\lambda|\mathbf{r}_0 - \mathbf{r}_{\text{LTT}}|}}{|\mathbf{r}_0 - \mathbf{r}_{\text{LTT}}|} \quad (1)$$

Here \mathbf{r}_{LTO} has to be summed over the sites occupied by the holes in the homogeneous phase or on the zig-zag stripes and \mathbf{r}_{LTT} over those in the static stripes. The factor x is the hole concentration and ΔE_c is thus the energy difference per Cu site. We have introduced the inverse Thomas Fermi screening length $\lambda \sim 1/(2a)$ of the order of the lattice spacing a . The sums are calculated using the mean distances of the holes $d_h = \sqrt{x}^{-1}$ in the homogeneous case and the mean distance between the stripes $d_s = (2x)^{-1}$ in units of the lattice spacing a (see Fig. 3). The distance within the static stripes is two lattice spacings.

The resulting energy differences are shown in Fig. 4. They vanish for small doping concentrations as well as at quarter filling. Then the stripes are so close that the configurations are close to equivalent. For intermediate doping the energy loss due to the charge condensation in the stripes gives minima at $0.05 < x < 0.1$ in agreement with the experimental situation. The suppression of the LTO-LTT transition can thus be explained by the Coulomb repulsion of the holes. This is consistent with the formation of the intermediate $Pccn$ phase in this doping regime.

The comparison of the position of the minima with the experimental data shows the best agreement with the picture of the formation of fluctuating stripes out of a uniform phase (solid line in Fig. 4). Notice though that for a lattice spacing of $a \approx 3.8 \text{ \AA}$ the energy scale is given by $10^{-2}e^2/a \approx 4 \times 10^{-2} \text{ eV}$. This is much too large in comparison with the enthalpy liberated across the transition, which is of the order of 10^{-4} eV per Cu site (see Fig. 5). The actual physical situation must thus be more involved.

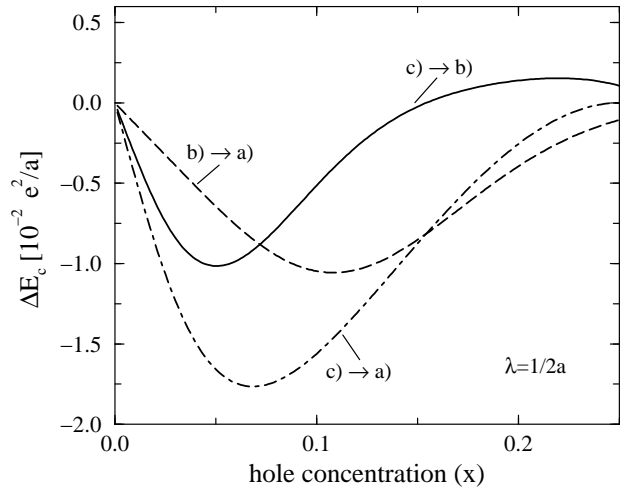


FIG. 4. Doping dependent differences of the Madelung energy per Cu site between the striped LTT phase and the two LTO configurations shown in Fig. 3. They are calculated according to Eq. (1). The energy is given in units of $10^{-2}e^2/a \approx 4 \cdot 10^{-2} \text{ eV}$. a is the lattice spacing. The positions of the minima are in qualitative agreement with the experimental LTO-LTT transition lines (Fig. 2).

III. ENTHALPY SCALING

For the samples shown in the phase diagram Fig. 1 specific heat measurements have been made. The area of the anomaly at the transition determines the entropy ΔS liberated at the transition.¹⁵ In Fig. 5 we have plotted the resulting enthalpy $\Delta H = T_{\text{LT}}\Delta S$ (filled symbols) as a function of the transition temperature T_{HT} of the HTT-LTO transition as shown in Fig. 1. The points all fall roughly of the same line, even though we analyzed different dopants varying both the Sr content x and the Nd or Eu concentration y . This implies a general relation between the HT and the LT transition and a common driving mechanism for the structural transitions.

Note that within the accuracy of the experiment the electron concentration in the CuO_2 planes does not play a crucial role for the value of ΔH . The $\text{La}_{1.85-y}\text{Nd}_y\text{Sr}_{0.15}\text{CuO}_4$ sample with constant hole doping (● in Fig. 5) follows the common line. This is consistent with the fact that structural phase transitions involving an octahedron tilt are common amongst perovskites.¹⁶

A. Landau theory

To obtain a phenomenological theoretical understanding we apply the standard Landau expansion of Gibb's free enthalpy in two order parameters:¹⁷

$$G = a(Q_1^2 + Q_2^2) + 2b(Q_1^4 + Q_2^4) + 4c Q_1^2 Q_2^2. \quad (2)$$

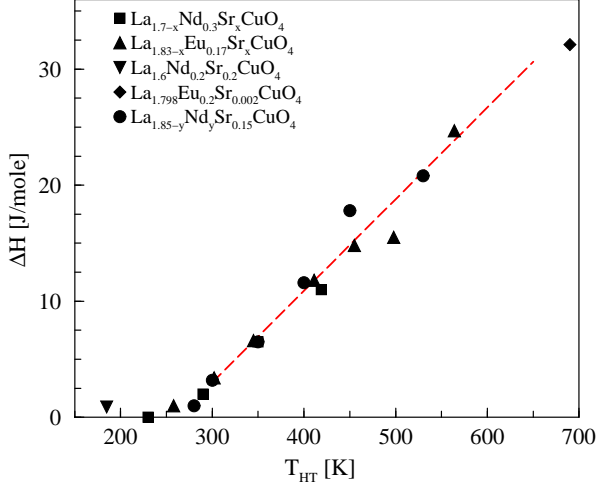


FIG. 5. Discontinuity of the enthalpy across the LT transition as a function of the corresponding T_{HT} . Full symbols are experimental values from specific heat measurements. The broken line is a guide to the eye.

The order parameters Q_1 and Q_2 measure the tilt of the CuO_6 octahedra about the $[110]_{\text{HTT}}$ and $[\bar{1}\bar{1}0]_{\text{HTT}}$ axis, respectively. The tilt axes are symmetric (lattice invariant under rotation of 90°), thus the coefficients are identical for both parameters. Since the tilt angle $\Phi < 5^\circ$ is small, we disregard higher then quartic terms. Applying the transformation $Q_1 = Q \cos \theta$ and $Q_2 = Q \sin \theta$ we obtain new order parameters Q measuring the size of the octahedron tilt angle Φ and the angle θ measuring the direction of the tilt with respect to the $[110]_{\text{HTT}}$ axis.

$$G = a Q^2 + b Q^4 + c Q^4 \sin^2(2\theta) \quad (3)$$

Above T_{LT} θ vanishes and G reduces to a single order parameter expansion. The change of sign of the second order coefficient induces the HTT-LTO transition with the transition temperature given by $a(T_{\text{HT}}) = 0$.

The temperature dependence of the order parameter in the LTO phase is usually expressed via

$$Q(T) = Q_0(T_{\text{HT}} - T)^\nu. \quad (4)$$

In a mean field picture we have $a(T) = a_0(T_{\text{HT}} - T)$, $b(T) = \text{const}$, and $\nu = 0.5$. The LTO-LTT transition is of first order induced by a jump of θ to a finite value of 45° . The transition temperature is determined by $c(T_{\text{LT}}) = 0$, i.e., the coefficient changes sign. For small Sr concentrations $x < 0.1$ in some samples the jump in θ is smaller and 45° are only reached after further cooling, giving rise to an intermediate $Pccn$ phase. Within this approach we neglect this effect. This is justified since the enthalpy discontinuity show in Fig. 5 was obtained by integrating over the whole specific heat anomaly down to the LTT regime.

The potential G is continuous across the transition but its derivative with respect to temperature is not, which leads to a discontinuity in the entropy.

$$\Delta S = \frac{\partial G}{\partial T} \Big|_{T=T_{\text{LT}}^+} - \frac{\partial G}{\partial T} \Big|_{T=T_{\text{LT}}^-} = \left[Q^4 \sin^2(2\theta) \frac{\partial c}{\partial T} \right]_{T=T_{\text{LT}}^-} \quad (5)$$

For this result we have assumed the derivatives $(\partial a)/(\partial T)$, $(\partial b)/(\partial T)$, and $(\partial Q)/(\partial T)$ to be continuous across the transition, and we used the fact that $c(T = T_{\text{LT}}^-) = 0$ and $\theta(T > T_{\text{LT}}) = 0$. For the discontinuity of the enthalpy we obtain

$$\Delta H = T_{\text{LT}} \Delta S = T_{\text{LT}} Q^4(T_{\text{LT}}) \frac{\partial c}{\partial T} \Big|_{T=T_{\text{LT}}^-}. \quad (6)$$

B. Determination of $Q(T)$

The temperature dependence of the octahedron tilt angle can be specified experimentally via the orthorhombic strain $(a - b) = Q^2 \sim \Phi^2$ as shown in Fig. 6. Here a and b are the lattice constants along the respective crystallographic axes determined by x-ray scattering. The full lines in Fig. 6 are given by the square of Eq. (4):

$$Q^2(T) = 0.00095 \frac{\text{\AA}}{\text{K}^{0.7}} (T_{\text{HT}} - T)^{0.7}. \quad (7)$$

For all samples we set $Q_0 = 0.031 \sqrt{\text{\AA}/\text{K}^{0.7}}$. In agreement with renormalization group studies¹⁸ an exponent of $2\nu = 0.7$ satisfactorily reproduces the experimental values above the saturation temperature $T^* \sim 150$ K to 200 K. Note that obtaining the universal prefactor Q_0 requires *not* to use reduced temperatures $(T_{\text{HT}} - T)/T_{\text{HT}}$ in Eq. (7).

For all samples the LTO-LTT transition temperature is well below the saturation temperature $T_{\text{LT}} < T^*$. To quantify the saturation behavior would require a systematic study of the saturation values of $Q(T \rightarrow 0)$ which has not been done. At $T = T_{\text{LT}}$ the deviation from the fit given by Eq. (7) is roughly of the same magnitude for all samples and as a simple approximation we introduce a constant correction term.

$$Q^2(T_{\text{LT}}) \approx 0.00095 \frac{\text{\AA}}{\text{K}^{0.7}} (T_{\text{HT}} - T_{\text{LT}})^{0.7} - 0.01 \text{\AA} \quad (8)$$

C. Comparison of theory and experiment

With the values of ν and Q_0 thus given and the data for T_{LT} and T_{HT} presented in Fig. 1 we calculate the theoretical values for the enthalpy from Eq. (6). The open symbols in Fig. 7 are the results calculating

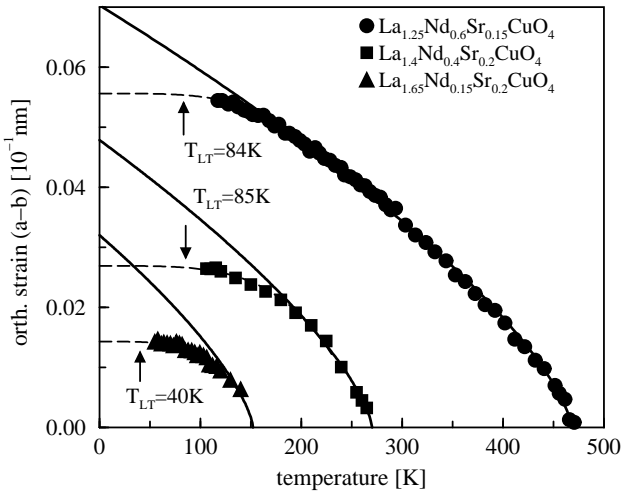


FIG. 6. Orthorhombic strain $(a - b) = Q^2 \sim \Phi^2$. a and b are the lattice constants along the respective crystallographic axes determined by x-ray scattering. The full lines are fits using Eq. (4) with $2\nu = 0.7$ and $Q_0 = 0.031 \sqrt{\text{Å}/\text{K}^{0.7}}$ for all samples. Broken lines are fits in the shape of $Q^2(T) = Q^2(0) (1 - \text{const } T^4)$ to match the order parameter saturation below $T^* \sim 150 \text{ K}$ to 200 K.

$Q(T_{\text{LT}})$ via Eq. (8). The scaling factor has been set to $(\partial c)/(\partial T)|_{T=T_{\text{LT}}^-} = 66 \text{ J}/(\text{mole K } \text{Å}^2)$. The black full symbols and broken lines in Figs. 5 and 7 are identical to allow a comparison with the directly measured values for ΔH . The inset in Fig. 7 shows a comparison between values obtained by via Eq. (8), open symbols, and those obtained without correction for saturation from Eq. (7), grey full symbols. The scaling factor for gray symbols has been set to $(\partial c)/(\partial T)|_{T=T_{\text{LT}}^-} = 41 \text{ J}/(\text{mole K } \text{Å}^2)$. In both cases the theoretical values show global scaling. The open symbols satisfactorily fall on the same line as the directly measured data given in Fig. 5. An exception is the large value for $\text{La}_{1.798}\text{Eu}_{0.2}\text{Sr}_{0.002}\text{CuO}_4$ which may be explained by an underestimated saturation of the order parameter or by a deviation of the prefactor Q_0 due to excess oxygen. We can thus conclude that the essential physics of the structural phase transition is captured by the Landau approach.

D. Thermal conductivity and superconductivity

The relation between lattice and electronic degrees of freedom has already been addressed in the context of thermal conductivity.⁴ As can be seen in the case of the $\text{Nd}_{0.3}$ samples in Fig. 5 the enthalpy anomaly becomes very small for a Sr content of $x \geq 0.17$. For $x \geq 0.17$ the anomaly of the thermal conductivity $\Delta\kappa$ across the LT transition also vanishes as shown in Ref. 4. Comparing Eq. (8) with the Sr dependence of the anomaly of

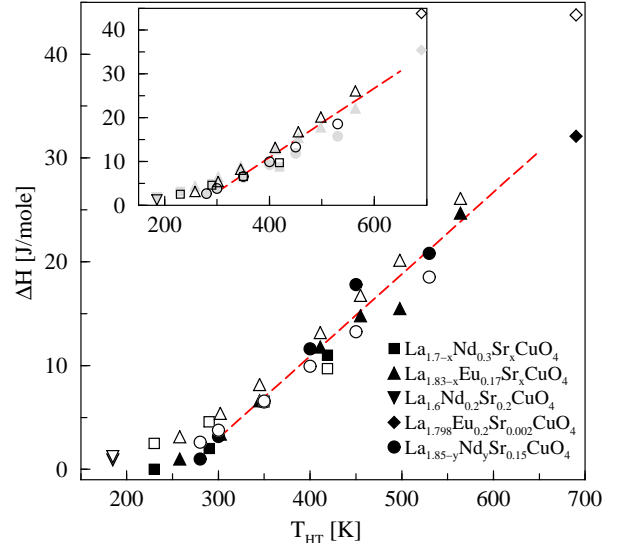


FIG. 7. Theoretical discontinuity of the enthalpy across the LT transition from Eq. (6) as a function of the corresponding T_{HT} . Open symbols in figure and inset are identical and are estimated using Eq. (8) for the order parameter, grey full symbols in the inset are obtained via Eq. (7). The black full symbols and broken lines are identical to those in Fig. 5 to allow for comparison.

the thermal conductivity $\Delta\kappa$,⁴ one can conclude that $\Delta\kappa$ is closely related to the octahedron tilt $\Delta\kappa \sim Q(T_{\text{LT}})$. The appearance of superconductivity in the LTT phase can equally be attributed to a small enough octahedron tilt order parameter¹⁴ and occurs in the $\text{Nd}_{0.3}$ samples also for $x \geq 0.17$. Thus the octahedron tilt angle and phononic and electronic transport properties are closely related.⁴

In $\text{La}_{2-x}\text{Sr}_x\text{CuO}_4$ without additional rare-earth doping, the Z -point phonon associated with the LTO-LTT transition softens only down to the temperature where superconductivity appears,¹⁹ underlining the electronic transport dependence on the crystal dynamics. A possible relation between the magnetic incommensurability and high-temperature lattice fluctuations has also been pointed out.¹⁹

IV. CONCLUSIONS

We have presented experimental data showing a universal characteristic minimum of the LTO-LTT transition temperature T_{LT} as a function of the Sr content of the sample independent of the Eu or Nd concentration. We have shown that the doping dependent maximum of the loss of Coulomb energy through the formation of charged stripes is a possible origin of the effect.

Analyzing specific heat measurements we have shown that the enthalpy jump at the LTO-LTT transition shows

universal scaling as a function of the HTT-LTO transition temperature. Within the variation of the results the scaling is independent of the electron concentration in the CuO₂ planes, showing that the structural transitions are essentially driven by the lattice dynamics. Results from a simple Landau expansion are consistent with the scaling behavior.

In conclusion our analysis of the LT transition does not unambiguously show the relevance of electronic degrees of freedom for this phase transition. Whereas the Sr-content dependence of T_{LT} suggests the influence of electronic properties, our discussion of the enthalpy reveals that the energy scale of the phase transition is basically determined by sterical lattice properties.

V. ACKNOWLEDGMENTS

R. Werner thanks C. Gros for discussions. The support of the DFG is gratefully acknowledged.

- ¹⁵ E. Gamper, Diploma thesis, University of Cologne, 1995.
- ¹⁶ A. D. Bruce and R. A. Cowley, *Structural Phase Transitions*, (Taylor & Francis, London, 1981).
- ¹⁷ J. D. Axe, A. H. Moudden, D. Hohlwein, D. E. Cox, K. M. Mohanty, A. R. Moodenbaugh, and Y. Xu, Phys. Rev. Lett. **62**, 2751 (1989).
- ¹⁸ M. Fisher, Rev. Mod. Phys. **46**, 597 (1974).
- ¹⁹ H. Kimura, K. Hirota, C. H. Lee, K. Yamada, and G. Shirane, J. Phys. Soc. Jpn. **69**, 851 (2000).

- ¹ J. M. Tranquada, B. J. Sternlieb, J. D. Axe, Y. Nakamura, and S. Uchida, Nature (London) **375**, 561 (1995); J. M. Tranquada, J. D. Axe, N. Ichikawa, Y. Nakamura, S. Uchida, and B. Nachumi, Phys. Rev. B **54**: 7489 (1996).
- ² M. v. Zimmermann, A. Vigliante, T. Niemöller, N. Ichikawa, T. Frello, J. Madsen, P. Wochner, S. Uchida, N. H. Andersen, J. M. Tranquada, D. Gibby, and J. R. Schneider, Europhys. Lett. **41**, 629 (1998).
- ³ T. Niemöller, N. Ichikawa, T. Frello, H. Hünnefeld, N. H. Andersen, S. Uchida, J. R. Schneider, and J. M. Tranquada, Eur. Phys. J. B **12**, 509 (1998).
- ⁴ O. Baberski, A. Lang, O. Maldonado, M. Hücker, B. Büchner, and A. Freimuth, Europhys. Lett. **44**, 335 (1998).
- ⁵ T. E. Mason, G. Aeppli, and H. A. Mook, Phys. Rev. Lett. **68**, 1414 (1992)
- ⁶ G. Shirane, R. J. Birgeneau, Y. Endoh, and M. A. Kastner, Physica B **197**, 158 (1994).
- ⁷ H. J. Schulz, J. Phys. (France), **50**, 2833 (1989).
- ⁸ J. Zaanen and O. Gunnarson, Phys. Rev. B **40**, 7391 (1989).
- ⁹ K. Yamada, C. H. Lee, Y. Endoh, G. Shirane, R. J. Birgeneau, and M. A. Kastner, Physica C **282-287**, 85 (1997).
- ¹⁰ J. Zaanen, M. L. Horbach, and W. van Saarloos, Phys. Rev. B **53**, 8671 (1996).
- ¹¹ J. D. Axe and M. K. Crawford, J. Low. Temp. Phys. **95**, 271 (1994).
- ¹² M. Breuer *et al.*, Physica C **208**, 217 (1993).
- ¹³ B. Büchner, M. Cramm, M. Braden, W. Braunisch, O. Hofels, W. Schnelle, R. Müller, A. Freimuth, W. Schlabitz, G. Heger, D. I. Khomskii, and D. Wolleben, Europhys. Lett. **21**, 953 (1993).
- ¹⁴ B. Büchner, M. Breuer, A. Freimuth, and A. P. Kampf, Phys. Rev. Lett. **73**, 1841 (1994).